Multi-element tomography: leveraging absorption and phase contrast in soft X-ray ptychography

Jayden Plumb[a*], Alexander Ditter[a], Dong-Hyun Kim[b], Kyubock Lee[b], Young-sang Yu[c] and David Shapiro[a]

[a]Advanced Light Source, Lawrence Berkeley National Laboratory, 6 Cyclotron Rd, Berkeley, CA, USA 94720; [b]Chungnam National University, 99 Daehak-ro, Yuseong District, Daejeon, South Korea 34134; [c]Chungbuk National University, 1 Chungdae-ro, Seowon-gu, Cheongju, Chungbuk, South Korea 28644

ABSTRACT

X-ray ptychography enables high-resolution imaging of multi-element systems by providing both optical density and phase contrast images. This study integrates few-energy ptychography with computed tomography to distinguish and spatially resolve nickel nanoparticles within a porous Al_2O_3 support. By leveraging contrast differences near a given absorption edge, our method achieves unambiguous 3D identification of an element using a single energy, significantly reducing acquisition time while maintaining nanoscale resolution. This approach is particularly valuable for studying catalytic processes, such as nanoparticle exsolution and dissolution in mesoporous alumina. High-resolution 3D imaging of these structures advances our understanding of catalytic dynamics, with implications for optimizing materials in environmental applications like dry reforming methane.

Keywords: X-ray ptychography, computed tomography, Ni-based catalysts, 3D imaging

1. INTRODUCTION

Soft X-ray ptychography is a coherent imaging technique widely used for the investigation of nanomaterials and organic samples [1,2]. X-ray ptychography is capable of producing images with spatial resolutions on the order of 10 nanometers, making it particularly valuable for probing the fine structure and elemental composition of micro-materials [1,3]. Typically, the technique involves imaging across multiple X-ray energies, which exploits the refractive behavior of elements near their absorption edges to enable the characterization of elemental or ionic distributions within a sample [4].

In many cases, three-dimensional (3D) information is desired, particularly when investigating anisotropic materials or processes. This is commonly addressed by combining ptychography with computed tomography, whereby a 3D volume is reconstructed from a series of 2D images acquired at different projection angles [5]. However, acquiring hundreds of projections significantly increases experimental time, which is a critical limitation at synchrotron radiation sources such as the Advanced Light Source (ALS) [6]. Upgrades to synchrotron facilities, such as the ALS-U project, predict an increase in coherence and photon flux, offering a potential reduction in experimental time [7]. Nevertheless, there remains a need to complement these advances by optimizing experimental protocols and automating data processing and analysis, as both ptychography and tomography are computationally intensive [8]. To address this, we have developed an analysis pipeline aimed at streamlining and accelerating the image reconstruction and analysis process.

Further challenges arise when elemental resolution is desired in combination with 3D imaging. Traditionally, this necessitates a full tomographic tilt series at multiple energies for each element of interest, further increasing the experimental time [5,9]. However, X-ray ptychography reconstructions produce two complementary datasets due to the real and imaginary parts of the refractive index: an image of phase contrast and an image of optical density, respectively [10]. This provides a unique opportunity to leverage the inverted relationship between these signals at elemental absorption edges to identify an element using a single-energy tilt series. Images taken near the absorption edge, produce a high optical density signal and a near-zero phase signal [11]. This approach has the potential to halve the experimental time required for elemental identification and further enable element-specific 3D characterization.

*jaydencplumb@gmail.com

X-Ray Nanoimaging: Instruments and Methods VII, edited by Yong S. Chu, Barry Lai,
Proc. of SPIE Vol. 13622, 1362203 · 2025 Published by SPIE
0277-786X · doi: 10.1117/12.3063920

Element-specific ptycho-tomography is of particular interest in the study of catalytic particles, composed of a porous alumina (Al_2O_3) matrix structure alloyed with various transition metals [12]. These particles have applications in the dry reforming of methane, during which the alloyed metals tend to precipitate out towards the surface [13]. Understanding the growth mechanisms of these metallic precipitates is crucial for catalyst design, and high-resolution 3D imaging with elemental resolution is ideally suited for this purpose [14].

2. METHODOLOGY

A ptycho-tomography experiment was conducted at the 7.0.1.2 COSMIC beamline at the Advanced Light Source, Lawrence Berkeley National Laboratory. The samples consisted of alumina particles with an average diameter of 1-1.5 μm, containing approximately 10% nickel alloyed throughout. These particles underwent controlled dissolution and exsolution cycling to precipitate nickel, simulating conditions relevant to catalytic operation. Soft X-ray ptychography was performed at the nickel L_3 absorption edge (~853 eV). A total of 156 projections were acquired over a limited angular range of approximately 135° in 0.9° steps; full 180° rotation was not possible due to sample mount geometry.

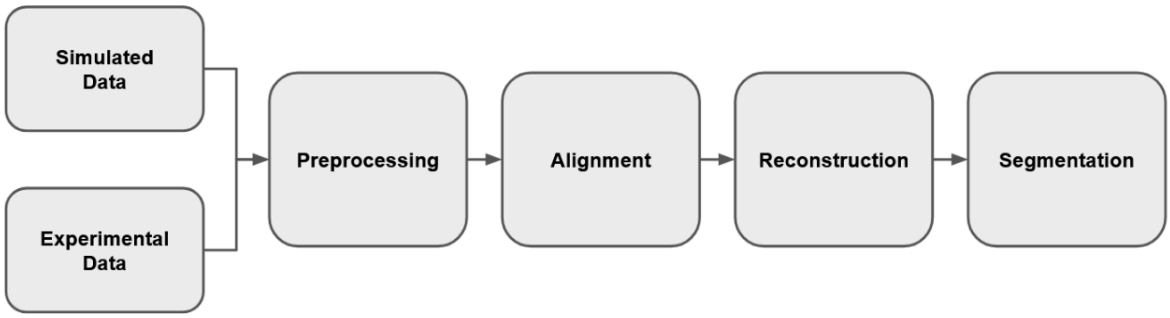

Figure 1. Analysis pipeline for reconstructing 3D volumes from ptycho-tomographic projections taken at COSMIC.

To validate the analysis pipeline and assess reconstruction fidelity, a simulated dataset was generated using multiple Shepp-Logan phantoms to represent individual particles, with additional metallic inclusions to mimic precipitated nickel particles. Forward projections were generated using a realistic model of the imaging geometry and included artificial jitter and noise to approximate experimental conditions. Once the experimental and simulated datasets were gathered, the analysis pipeline (see Figure 1) began with some basic preprocessing, including background subtraction and cropping. The next step is image alignment, which is critical to minimize reconstruction artifacts. Here, the rotational alignment consisted of pure translations determined from each image's centroid. An asymmetric object that remains in the field-of-view throughout rotation will demonstrate a centroid that oscillates sinusoidally in the direction perpendicular to the rotation axis. Image registration improves reconstruction quality and compensates for inherent misalignments in the experimental setup.

Next, a reconstruction of the 3D volume can be performed using direct or iterative algorithms, with a preference for iterative methods due to their robustness against limited-angle artifacts. This dataset was reconstructed using a model-based iterative reconstruction (MBIR) algorithm implemented in Python. Following reconstruction, individual slices were segmented to highlight metallic nickel precipitates. Segmentation was performed by assessing the optical density and phase contrast reconstructions: regions with high optical density and low phase contrast edge were identified as probable locations of nickel-rich particles.

3. RESULTS AND DISCUSSION

The experimental 3D reconstruction resulted in a volume of approximately 4.8 μm^3, containing ten distinct alumina particles. Figure 2 presents a representative slice from the reconstructed volume, illustrating the segmentation process. The segmentation workflow proceeds in three steps: (1) identification of high-value regions in the optical density image, (2) detection of local minima in the phase contrast image, and (3) determination of intersecting regions that satisfy both

criteria. This intersection highlights areas with high absorption and minimal phase shift, corresponding to the expected behavior of nickel at the absorption edge.

High optical density regions are indicative of metallic particles, which exhibit much greater absorption compared to the surrounding ceramic matrix. However, the presence of other metallic elements or impurities could confound identification based solely on absorption. The phase contrast signal, which theoretically exhibits a pronounced dip before approaching zero near the elemental absorption edge, serves as an additional discriminator. Local minima, or valleys in the phase contrast image also correspond to voids in the porous structure, confounding identification based solely on scattering. Thus, the intersection of high optical density and low phase contrast regions provides a robust method for identifying nickel-rich precipitates. The particle shown in Figure 2 demonstrates the segmentation process identifying 7 regions that are likely nickel nanoparticles. Other high-density regions that are not identified could be explained by varying Ni concentrations throughout the matrix or other metallic impurities.

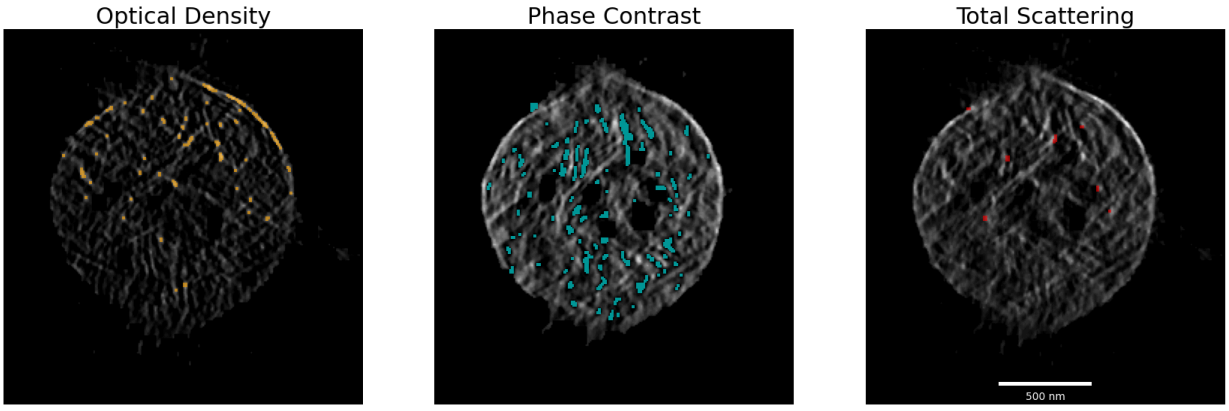

Figure 2. Tomography slices from 3D tomographic reconstructions of an Al_2O_3 catalyst particle with highlighted areas illustrating the segmentation process for identifying Ni nanoparticles. (left) Slice from the optical density reconstruction with high-density areas highlighted in orange. (middle) Slice from the phase contrast reconstruction with local minima highlighted in cyan. (right) Slice from the total scattering (i.e. optical density + phase) reconstruction that highlights the intersection of the previous two highlighted regions in red.

Artifacts arising from the limited angular range are evident near the top and bottom edges of the reconstructed particle, manifesting as blurring and streak artifacts. These inconsistencies, particularly near the particle boundaries, warrant caution in quantitative interpretation of those regions. Qualitatively, the segmentation results demonstrate good correspondence between the expected and observed locations of nickel precipitates. Ongoing analysis aims to extend these preliminary 2D findings to the full 3D volume, followed by an extraction of quantitative metrics such as volume fraction, size distribution, and spatial distribution of metallic inclusions. While these results focus on the identification of a single element (nickel), future work will expand this approach to multi-element systems by acquiring single-energy tilt series at the respective absorption edges of each metal of interest (e.g., cobalt or iron). This methodology holds promise for efficient, high-resolution, and element-specific 3D characterization of complex microscale materials.

ACKNOWLEDGEMENTS

The authors acknowledge support from the STROBE National Science Foundation Science & Technology Center, Grant No. DMR-1548924. This research used resources of the Advanced Light Source, a U.S. DOE Office of Science User Facility under contract no. DE-AC02-05CH11231.

REFERENCES

[1] D. A. Shapiro, Y. S. Yu, T. Tyliszczak, J. Cabana, R. Celestre, W. Chao, K. Kaznatcheev, A. L. D. Kilcoyne, F. Maia, S. Marchesini, Y. S. Meng, T. Warwick, L. L. Yang and H. A. Padmore, "Chemical composition mapping with

nanometre resolution by soft X-ray microscopy," Nature Photonics 8(10), 765–769 (2014). https://dx.doi.org/10.1038/nphoton.2014.207
[2] J. Miao, T. Ishikawa, Q. Shen and T. Earnest, "Extending X-ray crystallography to allow the imaging of noncrystalline materials, cells, and single protein complexes," Annu. Rev. Phys. Chem., 59(1), 387-410 (2008). https://doi.org/10.1146/annurev.physchem.59.032607.093642
[3] A. Maiden, G. Morrison, B. Kaulich, A. Gianoncelli and J. M. Rodenburg, "Soft X-ray spectromicroscopy using ptychography with randomly phased illumination," Nature Communications 4, 1669 (2013). https://doi.org/10.1038/ncomms2640
[4] A. Diaz, P. Trtik, M. Guizar-Sicairos, A. Menzel, P. Thibault and O. Bunk, "Quantitative X-ray phase nanotomography," Physical Review B—Condensed Matter and Materials Physics, 85(2), 020104 (2012). https://doi.org/10.1103/PhysRevB.85.020104
[5] M. Holler, M. Guizar-Sicairos, E.H.R. Tsai, R. Dinapoli, E. Müller, O. Bunk, J. Raabe and G. Aeppli, "High-resolution non-destructive three-dimensional imaging of integrated circuits," Nature 543, 402–406 (2017). https://doi.org/10.1038/nature21698
[6] T. Feggeler, A. Levitan, M. A. Marcus, H. Ohldag and D. A. Shapiro, "Scanning transmission X-ray microscopy at the Advanced Light Source," Journal of Electron Spectroscopy and Related Phenomena, 267, 147381 (2023). https://doi.org/10.1016/j.elspec.2023.147381
[7] C. Steier, P. Amstutz, K. Baptiste, P. Bong, E. Buice, P. Casey, K. Chow, R. Donahue, M. Ehrlichman, J. Harkins, T. Hellert, M. Johnson, J. Y. Jung, S. Leemann, R. Leftwich-Vann, D. Leitner, T. Luo, O. Omolayo, J. Osborn, G. Penn, G. Portmann, D. Robin, F. Sannibale, S. De Santis, C. Sun, C. Swenson, M. Venturini, S. Virostek, W. Waldron and E. Wallen, "Design progress of ALS-U, the soft x-ray diffraction limited upgrade of the advanced light source," In 10th International Particle Accelerator Conference (IPAC'19), Melbourne, Australia (2019). DOI: 10.18429/JACoW-IPAC2019-TUPGW097
[8] X. Yu, V. Nikitin, D. J. Ching, S. Aslan, D. Gürsoy and T. Biçer, "Scalable and accurate multi-GPU-based image reconstruction of large-scale ptychography data," Sci Rep 12, 5334 (2022). https://doi.org/10.1038/s41598-022-09430-3
[9] D. Gürsoy, F. De Carlo, X. Xiao, C.T. Jacobsen, "TomoPy: a framework for the analysis of synchrotron tomographic data," Synchrotron Radiation, 21(5), 1188-1193 (2014). https://doi.org/10.1107/S1600577514013939
[10] P. Thibault, M. Dierolf, A. Menzel, O. Bunk, C. David and F. Pfeiffer, "High-resolution scanning X-ray diffraction microscopy," Science, 321(5887), 379-382 (2008). https://dx.doi.org/10.1126/science.1158573
[11] A. P. Hitchcock, "Soft X-ray spectromicroscopy and ptychography," Journal of Electron Spectroscopy and Related Phenomena, 200, 49-63 (2015). https://doi.org/10.1016/j.elspec.2015.05.013
[12] A. B. Askari, M. al Samarai, B. Morana, L. Tillmann, N. Pfänder, A. Wandzilak, B. Watts, R. Belkhou, M. Muhler and S. DeBeer, "In Situ X-ray Microscopy Reveals Particle Dynamics in a NiCo Dry Methane Reforming Catalyst under Operating Conditions," ACS catalysis, 10(11), 6223-6230 (2020). https://doi.org/10.1021/acscatal.9b05517
[13] L. Wang and F. Wang, "Design Strategy, Synthesis, and Mechanism of Ni Catalysts for Methane Dry Reforming Reaction: Recent Advances and Future Perspectives," Energy & Fuels, 36(11), 5594-5621 (2022). https://doi.org/10.1021/acs.energyfuels.2c01007
[14] A. M. Wise, J. N. Weker, S. Kalirai, M. Farmand, D. A. Shapiro, F. Meirer and B. M. Weckhuysen, "Nanoscale Chemical Imaging of an Individual Catalyst Particle with Soft X-ray Ptychography," ACS catalysis, 6(4), 2178-2181 (2016). https://doi.org/10.1021/acscatal.6b00221